



HAL
open science

Finite element modelling of hybrid active–passive vibration damping of multilayer piezoelectric sandwich beams - part I: Formulation

Marcelo A. Trindade, Ayeche Benjeddou, Roger Ohayon

► To cite this version:

Marcelo A. Trindade, Ayeche Benjeddou, Roger Ohayon. Finite element modelling of hybrid active–passive vibration damping of multilayer piezoelectric sandwich beams - part I: Formulation. International Journal for Numerical Methods in Engineering, 2001, 51 (7), pp.835-854. 10.1002/nme.189 . hal-03179654

HAL Id: hal-03179654

<https://hal.science/hal-03179654>

Submitted on 1 Sep 2023

HAL is a multi-disciplinary open access archive for the deposit and dissemination of scientific research documents, whether they are published or not. The documents may come from teaching and research institutions in France or abroad, or from public or private research centers.

L'archive ouverte pluridisciplinaire **HAL**, est destinée au dépôt et à la diffusion de documents scientifiques de niveau recherche, publiés ou non, émanant des établissements d'enseignement et de recherche français ou étrangers, des laboratoires publics ou privés.

Finite element modelling of hybrid active–passive vibration damping of multilayer piezoelectric sandwich beams—part I: Formulation

M. A. Trindade^{*,†}, A. Benjeddou and R. Ohayon

*Structural Mechanics and Coupled Systems Laboratory, Conservatoire National des Arts et Métiers,
2, rue Conté, 75003 Paris, France*

This work, in two parts, proposes, in this first part, an electromechanically coupled finite element model to handle active–passive damped multilayer sandwich beams, consisting of a viscoelastic core sandwiched between layered piezoelectric faces. The latter are modelled using the classical laminate theory, whereas the face/core/face system is modelled using classical three-layers sandwich theory, assuming Euler–Bernoulli thin faces and a Timoshenko relatively thick core. The frequency-dependence of the viscoelastic material is handled through the anelastic displacement fields (ADF) model. To make the control system feasible, a modal reduction is applied to the resulting ADF augmented system. Validation of the approach developed in this part is presented in Part 2 of the paper together with the hybrid damping performance analysis of a cantilever beam.

KEY WORDS: finite element; multilayer sandwich beam; piezoelectric material; viscoelastic material; active–passive vibration damping

INTRODUCTION

Since the mid 1980s, researches for new vibration control systems have been directed to hybrid active–passive control strategies. These were mainly based on simultaneous use of piezoelectric and viscoelastic materials in the same damping treatment. In particular, it was found [1] that, during the last 6 years, these researches have focused on configurations that augment the damping ability of the conventional passive constrained layer damping (PCLD) treatments. Depending on the position of the piezoelectric actuator, the passive and active actions can operate either separately or simultaneously. In the former configuration, the passive constrained layer and piezoelectric patches are placed away from each other, so that each

*Correspondence to: M. A. Trindade, Structural Mechanics and Coupled Systems Laboratory, Conservatoire National des Arts et Métiers, 2, rue Conté, 75003 Paris, France

†E-mail: trindade@cham.fr

Contract/grant sponsor: Délégation générale pour l'Armement; contract/grant number: D.G.A./D.S.P./S.T.T.C./MA. 97-2530

Contract/grant sponsor: CAPES; contract/grant number: BEX 2494/95-7.

of them uses independently its own damping mechanism. That is, the piezoelectric actuator uses the conventional active control (AC) mechanism, based on induced in-plane piezoelectric actuation strains; whereas, the passive constrained layer uses its conventional passive damping mechanism, based on vibratory energy dissipation through transverse shear strains induced in the viscoelastic material by relative in-plane displacements of the constraining layer and base structure. Such configuration is then called AC/PCLD treatment. Moreover, combined active and passive control actions can be obtained by replacing the passive constraining layer by an active piezoelectric layer. This is the so-called active constrained layer damping (ACL D) treatment. Here, the active constraining layer tends to augment the relative in-plane displacements in order to increase the relative shear in the viscoelastic core. Hence, more dissipation and damping can be obtained. Thus, the ACL D uses the same damping mechanism as the PCLD. This is also the mechanism of the configurations where the piezoelectric actuator is bonded to the upper surface of the constraining layer.

Review of hybrid damping configurations proposed in the literature can be found in References [1, 2]. Although these hybrid damping constructions vary from three up to seven layers, they were mainly modelled using the classical three-layer sandwich theory. This was made using several simplifying assumptions. Hence, Baz and Ro [3] have reduced a four-layer ACL D beam into a three-layer one by assuming the piezoelectric sensor and base beam as an equivalent single layer in order to formulate a specific two-node sandwich finite element. Later, the previous element was adapted by Crassidis, Baz and Wereley [4] to model a five-layers hybrid beam which was reduced to a three-layer construction by considering the base beam and the attached piezoelectric sensor and actuator on its upper and lower surfaces, respectively, as a single layer. Recently, the extension and flexure motions of a seven-layers hybrid damped beam were modelled separately using a Rayleigh–Ritz approach by Rongong *et al.* [5]. Here, the strains of the constraining layer and the bonded piezoelectric actuator on its upper surface were supposed compatible. Four-layer hybrid beam configurations were also analysed without reduction of the number of layers. Chen and Baz [6] have discretized each layer of the construction using three-dimensional finite elements. In particular, for the piezoelectric layers, additional electric potential degrees of freedom were necessary to take into account the piezoelectric effect. However, Lam *et al.* [7] have used the Rayleigh–Ritz approach to compare various three- and four-layer hybrid AC/PCLD beam configurations. Nevertheless, no models have been presented for other than piezoelectric and passive constraining layer patches attached on the same side of the beam; that is for three-layer construction only.

In a previous work [8], a finite element model was proposed by the present authors to handle piezoelectric sandwich beams. To solve shear locking phenomena of this model, its kinematics parametrization was then modified in Reference [9] leading to a shear locking free electromechanically coupled finite element model. In the present work, this sandwich beam model [9] is extended to account for multilayer sandwich beams, consisting of a viscoelastic core sandwiched between layered piezoelectric faces. The latter are modelled using the classical laminate theory, whereas classical sandwich theory is considered for the face/core/face beam, assuming Euler–Bernoulli hypotheses for the faces and Timoshenko ones for the core. The anelastic displacement fields (ADF) model, developed by Lesieutre and Bianchini [10], is used to handle the frequency-dependence of the viscoelastic material. The latter was preferred to that of Golla–Hughes–McTavish (GHM), because the former has less material parameters and leads to smaller system according to a recent comparison made by Trindade *et al.* [11]. Then, a complex-basis model reduction of the augmented system is proposed and applied to

the active–passive constrained optimal control of sandwich damped beams. The control gains are provided by an LQR control law with limited control voltage and restricted beam tip deflection, in order to respect the model assumptions. After its validation, achieved in the Part 2 of this paper, the new finite element is used to study the active control of a sandwich cantilever beam with viscoelastic core through a pair of attached piezoelectric actuators. The hybrid damping performance of the five-layer configuration is studied for viscoelastic layer thickness and actuator length variations.

The specific two-node sandwich finite element with layered faces containing piezoelectric actuator patches, the modal reduction of the augmented ADF viscoelastic model, and the piezoelectric active control of sandwich damped beam configuration are the main originalities of the present work. In what follows, a theoretical variational formulation of the problem is presented and then used to develop the electromechanically coupled finite element model of multilayer sandwich beams. Next, the ADF model is briefly presented to account for the frequency-dependence of the viscoelastic core properties. An elastic–piezoelectric–viscoelastic coupled state-space model is then constructed, reduced and applied to an optimal LQR controller design.

THEORETICAL FORMULATION

A sandwich beam made of laminate faces, with elastic and/or piezoelectric sublayers, and viscoelastic core is considered. Therefore, faces are modelled using classical laminate theory and the whole beam is modelled using classical sandwich theory. Euler–Bernoulli assumptions are considered for the laminate faces, whereas those of Timoshenko are retained for the viscoelastic core. The piezoelectric layers are supposed transversely poled and subject to transverse electrical fields. Elastic and viscoelastic layers are assumed insulated. All layers are assumed perfectly bonded and in plane stress state. The length, width and thickness of the beam are denoted by L , b and h , respectively. The subscripts a_j , b_j and c refer to quantities relative to the j th sublayer of upper a and lower b faces and to the core, respectively. Detailed nomenclature is presented in Appendix C.

Kinematics

Axial displacements $\check{u}_i(x, y, z)$ of the i th layer are assumed linear through thickness, whereas transverse ones $\check{w}_i(x, y, z)$ are supposed constant

$$\begin{aligned}\check{u}_i(x, y, z) &= u_i(x) + (z - z_i)\beta_i(x), \quad i = a, b, c \\ \check{w}_i(x, y, z) &= w(x)\end{aligned}\tag{1}$$

The kinematic description of the sandwich beam is presented in Figure 1. Notice that the same displacement fields u_k ($k = a, b$) are considered for all sublayers k_j of the face k . From Euler–Bernoulli hypotheses, $\beta_k = \beta = -w'$ ($k = a, b$), where, \bullet' is used to denote $\partial \bullet / \partial x$. The mid-plan of the core is set to coincide with the origin of the z -axis, so that $z_c = 0$. Let us define the mean and relative axial displacements of the laminate faces \bar{u} and \tilde{u} as (Figure 1)

$$\bar{u} = \frac{u_a + u_b}{2}, \quad \tilde{u} = u_a - u_b\tag{2}$$

cores and thick faces and decreases for the opposite case. The parameter λ vanishes only for a single Timoshenko core, i.e. without covering face layers.

A constant transverse electrical field is assumed for the piezoelectric layers and the remaining in-plane components are supposed to vanish. Although electrostatic equilibrium equation is only satisfied with a linear electrical field assumption [8, 12], it was found that the linear part is negligible for the problems treated in this work. Consequently it is, for the k_j th face piezoelectric sublayer,

$$E_{3k_j} = -\frac{V_{k_j}}{h_{k_j}} \quad (5)$$

where V_{k_j} is the difference of electric potential of the k_j th laminae, defined by $V_{k_j} = V_{k_j}^+ - V_{k_j}^-$, where $V_{k_j}^+$ and $V_{k_j}^-$ are the voltages applied on the upper and lower skins of the k_j th face piezoelectric sublayer.

Reduced constitutive equations

Linear orthotropic piezoelectric materials with material symmetry axes parallel to those of the beam are considered. c_{ij} , e_{lj} and ϵ_{ll} ($i, j = 1, \dots, 6$; $l = 1, 2, 3$) denote their elastic, piezoelectric and dielectric constants. For simplicity of notation, all layers will be considered piezoelectric. Elastic and viscoelastic layers are obtained by making their piezoelectric constants vanish. The three-dimensional linear constitutive equations of an orthotropic piezoelectric layer can be reduced to (for details of this reduction, see Reference [8])

$$\begin{aligned} \sigma_1 &= c_{11}^* \epsilon_1 - e_{31}^* E_3, & \sigma_{5c} &= c_{55}^c \epsilon_{5c} \\ D_3 &= e_{31}^* \epsilon_1 + \epsilon_{33}^* E_3 \end{aligned} \quad (6)$$

where

$$c_{11}^* = c_{11} - \frac{c_{13}^2}{c_{33}}, \quad e_{31}^* = e_{31} - \frac{c_{13}}{c_{33}} e_{33}, \quad \epsilon_{33}^* = \epsilon_{33} + \frac{e_{33}^2}{c_{33}}$$

σ_1 , σ_5 and D_3 are axial and shear stress components and transverse electrical displacement. Notice that electromechanical coupling in the piezoelectric face sublayers is between axial strain and transverse electrical field. This is the conventional piezoelectric extension actuation mechanism. Its static actuation and control performances were compared with those of the shear actuation mechanism in References [13, 14].

Variational formulation

Using d'Alembert's principle, the following variational equation can be written for the piezoelectric layered faces sandwich beam:

$$\delta T - \delta H + \delta W = 0, \quad \forall \delta \tilde{u}, \delta \tilde{w}, \delta V_{k_j} \quad (7)$$

where δT , δH and δW are the virtual work of inertial, electromechanical internal and applied mechanical forces, respectively.

The electromechanical internal forces virtual work of the layered piezoelectric faces sandwich beam is

$$\delta H = \delta H_c + \sum_{k=a}^b \sum_{j=1}^{n,m} \delta H_{k_j} \quad (8)$$

where

$$\delta H_{k_j} = \int_{\Omega_{k_j}} (\sigma_{1k_j} \delta \varepsilon_{1k} - D_{3k_j} \delta E_{3k_j}) d\Omega_{k_j}, \quad \delta H_c = \int_{\Omega_c} (\sigma_{1c} \delta \varepsilon_{1c} + \sigma_{5c} \delta \varepsilon_{5c}) d\Omega_c$$

with Ω_{k_j} and Ω_c being the volume of the k_j th sublayer and the core, respectively.

Using constitutive equations (6), strain (4) and electrical field (5) relations, then integrating through thickness, the above equations, for the k_j th face piezoelectric sublayer and elastic core, become

$$\begin{aligned} \delta H_{k_j} = & \int_0^L \left[c_{11}^{*k_j} (A_{k_j} \delta \varepsilon_k^m \varepsilon_k^m + \bar{I}_{k_j} \delta \varepsilon_k^m \varepsilon_k^b + \bar{I}_{k_j} \delta \varepsilon_k^b \varepsilon_k^m + I_{k_j} \delta \varepsilon_k^b \varepsilon_k^b) + e_{31}^{*k_j} (A_{k_j} \delta \varepsilon_k^m + \bar{I}_{k_j} \delta \varepsilon_k^b) \frac{V_{k_j}}{h_{k_j}} \right. \\ & \left. + e_{31}^{*k_j} \frac{\delta V_{k_j}}{h_{k_j}} (A_{k_j} \varepsilon_k^m + \bar{I}_{k_j} \varepsilon_k^b) - \epsilon_{33}^{*k_j} A_{k_j} \frac{\delta V_{k_j}}{h_{k_j}} \frac{V_{k_j}}{h_{k_j}} \right] dx \quad (9) \\ \delta H_c = & \int_0^L (c_{11}^{*c} A_c \delta \varepsilon_c^m \varepsilon_c^m + c_{11}^{*c} I_c \delta \varepsilon_c^b \varepsilon_c^b + k_c c_{55}^c A_c \delta \varepsilon_c^s \varepsilon_c^s) dx \end{aligned}$$

where k_c is the shear correction factor. Notice that here, unlike in the three-layer sandwich beam model of Reference [9], there are membrane-bending coupling terms due to the multilayer characteristic of the faces. A_{k_j} , \bar{I}_{k_j} and I_{k_j} are, respectively, the area and the first and second moments of inertia of the k_j th face sublayer cross-section. These are

$$[A_{k_j}, \bar{I}_{k_j}, I_{k_j}] = \int_{-b/2}^{b/2} \int_{z_{k_j}-h_{k_j}/2}^{z_{k_j}+h_{k_j}/2} [1, (z - z_k), (z - z_k)^2] dz dy \quad (10)$$

where the local z -axis of the k_j th sublayer is situated at

$$z_{k_j} = \pm \frac{h_{k_j} + h_c}{2} \pm \sum_{r=1}^{j-1} h_{k_r}, \quad k = a(+), b(-)$$

One may notice from (9) that for an applied difference of potential V_{k_j} on the k_j th face piezoelectric sublayer, the variations δV_{k_j} vanish, in the last two terms of δH_{k_j} , and its second term results in the virtual work $\delta H_{k_j,me}$ of a generalized piezoelectric load equivalent to

$$\delta H_{k_j,me} = - \int_0^L e_{31}^{*k_j} (A_{k_j} \delta \varepsilon_k^m + \bar{I}_{k_j} \delta \varepsilon_k^b) \frac{V_{k_j}}{h_{k_j}} dx \quad (11)$$

when moved to the right-hand side of (7). For homogeneous properties in the axial direction, according to (4), this may also be expressed as the virtual work of boundary generalized piezoelectric loads,

$$\delta H_{k_j,me} = -e_{31}^{*k_j} \left[A_{k_j} \left(\delta \bar{u} \pm \frac{\delta \bar{u}}{2} \right) - \bar{I}_{k_j} \delta w' \right]_0^L \frac{V_{k_j}}{h_{k_j}} \quad (12)$$

The last term of (12) means that the piezoelectric layers may induce bending on the sandwich beam due to layered faces asymmetry, unlike for single layer faces [9].

The inertial forces virtual work of the layered faces sandwich beam is

$$\delta T = \delta T_c + \sum_{k=a}^b \sum_{j=1}^{n,m} \delta T_{k_j} \quad (13)$$

where

$$\delta T_{k_j} = - \int_{\Omega_{k_j}} [\rho_{k_j}(\delta \ddot{u}_k \ddot{u}_k + \delta \ddot{w} \ddot{w})] d\Omega_{k_j}, \quad \delta T_c = - \int_{\Omega_c} [\rho_c(\delta \ddot{u}_c \ddot{u}_c + \delta \ddot{w} \ddot{w})] d\Omega_c$$

with ρ_i being the volumic mass density of the i th layer and $\dot{\bullet}$ states for $\partial \bullet / \partial t$.

Using the displacements relations (1) and (3), and integrating through thickness, the above equations become

$$\begin{aligned} \delta T_{k_j} &= - \int_0^L \rho_{k_j} [A_{k_j}(\delta u_k \ddot{u}_k + \delta w \ddot{w}) - \bar{I}_{k_j}(\delta u_k \ddot{w}' + \delta w' \ddot{u}_k) + I_{k_j} \delta w' \ddot{w}'] dx \\ \delta T_c &= - \int_0^L \rho_c [A_c(\delta u_c \ddot{u}_c + \delta w \ddot{w}) + I_c \delta \beta_c \ddot{\beta}_c] dx \end{aligned} \quad (14)$$

Notice that, due to the multilayer characteristic of the faces, there are translation–rotation inertial coupling terms.

The beam is subjected to surface axial and transversal forces at the boundaries of each face sublayer ($F_x^{k_j}$, $F_z^{k_j}$) and core (F_x^c , F_z^c), and to body ones ($f_x^{k_j}$, $f_z^{k_j}$, f_x^c , f_z^c). Their virtual work on the beam can be written as

$$\delta W = \sum_{i=a}^c \delta W_i \quad (15)$$

where

$$\begin{aligned} \delta W_k &= \sum_{j=1}^{n,m} \left\{ \left[\int_{A_{k_j}} (F_x^{k_j} \delta \ddot{u}_k + F_z^{k_j} \delta w) dA_{k_j} \right]_0^L + \int_{\Omega_{k_j}} (f_x^{k_j} \delta \ddot{u}_k + f_z^{k_j} \delta w) d\Omega_{k_j} \right\} \\ \delta W_c &= \left[\int_{A_c} (F_x^c \delta \ddot{u}_c + F_z^c \delta w) dA_c \right]_0^L + \int_{\Omega_c} (f_x^c \delta \ddot{u}_c + f_z^c \delta w) d\Omega_c \end{aligned}$$

Using displacement expressions (1), one may write the previous equation for the k th face and the core as

$$\begin{aligned} \delta W_k &= [N_k \delta u_k - M_k \delta w' + Q_k \delta w]_0^L + \int_0^L (n_k \delta u_k - m_k \delta w' + q_k \delta w) dx \\ \delta W_c &= [N_c \delta u_c + M_c \delta \beta_c + Q_c \delta w]_0^L + \int_0^L (n_c \delta u_c + m_c \delta \beta_c + q_c \delta w) dx \end{aligned} \quad (16)$$

where the, boundary and distributed, normal, moment and shear resultants are defined as

$$N_k = \sum_j N_{k_j}, \quad M_k = \sum_j M_{k_j}, \quad Q_k = \sum_j Q_{k_j}, \quad n_k = \sum_j n_{k_j}, \quad m_k = \sum_j m_{k_j}, \quad q_k = \sum_j q_{k_j} \quad (17)$$

with

$$\begin{aligned}
N_{k_j} &= \int_{A_{k_j}} F_x^{k_j} dA_{k_j}, & n_{k_j} &= \int_{A_{k_j}} f_x^{k_j} dA_{k_j} \\
M_{k_j} &= \int_{A_{k_j}} F_x^{k_j} (z - z_k) dA_{k_j}, & m_{k_j} &= \int_{A_{k_j}} f_x^{k_j} (z - z_k) dA_{k_j} \\
Q_{k_j} &= \int_{A_{k_j}} F_z^{k_j} dA_{k_j}, & q_{k_j} &= \int_{A_{k_j}} f_z^{k_j} dA_{k_j} \\
N_c &= \int_{A_c} F_x^c dA_c, & n_c &= \int_{A_c} f_x^c dA_c \\
M_c &= \int_{A_c} F_x^c z dA_c, & m_c &= \int_{A_c} f_x^c z dA_c \\
Q_c &= \int_{A_c} F_z^c dA_c, & q_c &= \int_{A_c} f_z^c dA_c
\end{aligned}$$

One may notice that the multilayer characteristic of the faces has no effect on the normal and transverse shear stress resultants N_k and Q_k , since they may be obtained by the sum of the forces corresponding to each sublayer. However, a difference between the axial forces $F_x^{k_j}$ ($j = 1, \dots, (n, m)$) of each sublayer of face k may induce a bending moment M_k . Similarly, the distributed forces $f_x^{k_j}$ ($j = 1, \dots, (n, m)$) may induce a distributed bending moment m_k . This membrane-bending coupling is equivalent to that observed for the piezoelectric action (12) due to the first moment of inertia \bar{I}_{k_j} .

FINITE ELEMENT FORMULATION

From the variational formulation and virtual work expressions presented in the last section, a finite element model was developed for the laminate faces adaptive sandwich beam. It assumes Lagrange linear shape functions for the mean and relative axial displacements, \bar{u} and \tilde{u} and Hermite cubic ones for the transverse deflection w . The difference of electric potentials V_{k_r} ($r = 1, \dots, (\hat{n}, \hat{m})$) of the \hat{n}, \hat{m} face piezoelectric sublayers are assumed constant in the element (Figure 2). This leads to the following elementary degrees of freedom (dof) column vector $\hat{\mathbf{q}}_e$ (cf. Appendix A):

$$\hat{\mathbf{q}}_e = \text{col}(\bar{u}_1, w_1, w'_1, \tilde{u}_1, \bar{u}_2, w_2, w'_2, \tilde{u}_2, V_{a_1e}, \dots, V_{a_{\hat{n}}e}, V_{b_1e}, \dots, V_{b_{\hat{m}}e}) \quad (18)$$

Based on this dof vector and relations (9), the discretized virtual work of the elementary electromechanical internal forces of the face sublayers $\delta H_{k_j}^e$ and the core δH_c^e are

$$\begin{aligned}
\delta H_{k_j}^e &= \delta \hat{\mathbf{q}}_e^T (\hat{\mathbf{K}}_{k_j m}^e - \hat{\mathbf{K}}_{k_j m e}^e - \hat{\mathbf{K}}_{k_j m e}^{e T} + \hat{\mathbf{K}}_{k_j e}^e) \hat{\mathbf{q}}_e = \delta \hat{\mathbf{q}}_e^T \hat{\mathbf{K}}_{k_j}^e \hat{\mathbf{q}}_e \\
\delta H_c^e &= \delta \hat{\mathbf{q}}_e^T \hat{\mathbf{K}}_c^e \hat{\mathbf{q}}_e
\end{aligned} \quad (19)$$

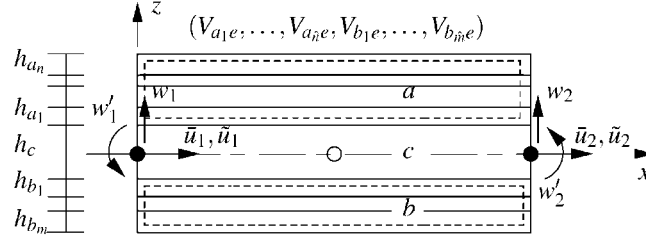


Figure 2. Piezoelectric laminated sandwich beam finite element.

where the elementary mechanical $\hat{\mathbf{K}}_{k,m}^e$, $\hat{\mathbf{K}}_c^e$, piezoelectric $\hat{\mathbf{K}}_{k,me}^e$ and dielectric $\hat{\mathbf{K}}_{k,e}^e$ stiffness matrices have the expressions

$$\begin{aligned}
\hat{\mathbf{K}}_{k,m}^e &= \int_0^{L_e} c_{11}^{*k_j} [A_{k_j} \mathbf{B}_{km}^T \mathbf{B}_{km} + \bar{I}_{k_j} (\mathbf{B}_{km}^T \mathbf{B}_{kb} + \mathbf{B}_{kb}^T \mathbf{B}_{km}) + I_{k_j} \mathbf{B}_{kb}^T \mathbf{B}_{kb}] dx \\
\hat{\mathbf{K}}_c^e &= \int_0^{L_e} [c_{11}^{*c} (A_c \mathbf{B}_{cm}^T \mathbf{B}_{cm} + I_c \mathbf{B}_{cb}^T \mathbf{B}_{cb}) + k_c c_{55}^c A_c \mathbf{B}_{cs}^T \mathbf{B}_{cs}] dx \\
\hat{\mathbf{K}}_{k,me}^e &= - \int_0^{L_e} e_{31}^{*k_j} \frac{1}{h_{k_j}} [A_{k_j} \mathbf{B}_{km}^T + \bar{I}_{k_j} \mathbf{B}_{kb}^T] \mathbf{N}_{pk_j} dx \\
\hat{\mathbf{K}}_{k,e}^e &= - \int_0^{L_e} \epsilon_{33}^{*k_j} \frac{A_{k_j}}{h_{k_j}^2} \mathbf{N}_{pk_j}^T \mathbf{N}_{pk_j} dx
\end{aligned} \tag{20}$$

with L_e being the element length. \mathbf{B}_{km} , \mathbf{B}_{cm} , \mathbf{B}_{kb} and \mathbf{B}_{cb} are the, faces (k) and core (c), membrane (m) and bending (b) strain operators. \mathbf{B}_{cs} is the core shear strain operator and, \mathbf{N}_{pk_j} is the difference of electric potential interpolation matrix (cf. Appendix A).

Similarly, the elementary inertial forces virtual work $\delta T_{k_j}^e$ and δT_c^e may be discretized as

$$\begin{aligned}
\delta T_{k_j}^e &= -\delta \hat{\mathbf{q}}_e^T (\hat{\mathbf{M}}_{k_j,t}^e - \hat{\mathbf{M}}_{k_j,tr}^e - \hat{\mathbf{M}}_{k_j,tr}^{eT} + \hat{\mathbf{M}}_{k_j,r}^e) \ddot{\mathbf{q}}_e = -\delta \hat{\mathbf{q}}_e^T \hat{\mathbf{M}}_{k_j}^e \ddot{\mathbf{q}}_e \\
\delta T_c^e &= -\delta \hat{\mathbf{q}}_e^T (\hat{\mathbf{M}}_{ct}^e + \hat{\mathbf{M}}_{cr}^e) \ddot{\mathbf{q}}_e = -\delta \hat{\mathbf{q}}_e^T \hat{\mathbf{M}}_c^e \ddot{\mathbf{q}}_e
\end{aligned} \tag{21}$$

where $\ddot{\mathbf{q}}_e$ is the elementary acceleration vector. From (14) and (18), the elementary mass matrices of the k_j th face sublayer and core are, respectively,

$$\begin{aligned}
\hat{\mathbf{M}}_{k_j,t}^e &= \int_0^{L_e} \rho_{k_j} A_{k_j} (\mathbf{N}_{kx}^T \mathbf{N}_{kx} + \mathbf{N}_z^T \mathbf{N}_z) dx, & \hat{\mathbf{M}}_{k_j,tr}^e &= \int_0^{L_e} \rho_{k_j} \bar{I}_{k_j} (\mathbf{N}_{kx}^T \mathbf{N}_{kr} + \mathbf{N}_{kr}^T \mathbf{N}_{kx}) dx \\
\hat{\mathbf{M}}_{k_j,r}^e &= \int_0^{L_e} \rho_{k_j} I_{k_j} \mathbf{N}_{kr}^T \mathbf{N}_{kr} dx \\
\hat{\mathbf{M}}_{ct}^e &= \int_0^{L_e} \rho_c A_c (\mathbf{N}_{cx}^T \mathbf{N}_{cx} + \mathbf{N}_z^T \mathbf{N}_z) dx, & \hat{\mathbf{M}}_{cr}^e &= \int_0^{L_e} \rho_c I_c \mathbf{N}_{cr}^T \mathbf{N}_{cr} dx
\end{aligned} \tag{22}$$

\mathbf{N}_{ix} , \mathbf{N}_z and \mathbf{N}_{ir} are the translation in x and z directions and rotation interpolation matrices (cf. Appendix A).

Since the point forces can be added *a posteriori* to the matricial system, the discretized elementary virtual work of applied mechanical forces reduces to

$$\delta W^e = \delta \hat{\mathbf{q}}_e^T \hat{\mathbf{F}}_m^e \quad (23)$$

where $\hat{\mathbf{F}}_m^e$ defines the vector of generalized distributed mechanical nodal forces obtained from (16),

$$\hat{\mathbf{F}}_m^e = \int_0^{L_e} [\mathbf{N}_{ax}^T n_a + \mathbf{N}_{bx}^T n_b + \mathbf{N}_{cx}^T n_c + \mathbf{N}_{az}^T (q_a + q_b + q_c) - \mathbf{N}_{ar}^T (m_a + m_b) + \mathbf{N}_{cr}^T m_c] dx \quad (24)$$

Assembling on the faces sublayers, then on the beam layers and using Equations (19), (21) and (23), the discretized variational equation (7) reduced to the element level can be written as

$$(\hat{\mathbf{M}}_f^e + \hat{\mathbf{M}}_c^e) \ddot{\hat{\mathbf{q}}}_e + (\hat{\mathbf{K}}_f^e + \hat{\mathbf{K}}_c^e) \hat{\mathbf{q}}_e = \hat{\mathbf{F}}_m^e \quad (25)$$

where $\hat{\mathbf{M}}_f^e = \sum_k \sum_j \hat{\mathbf{M}}_{kj}^e$ and $\hat{\mathbf{K}}_f^e = \sum_k \sum_j \hat{\mathbf{K}}_{kj}^e$. One may notice that, since electrical dofs inertia vanishes, mechanical and electrical dofs are coupled statically only (time-independent relationship). Therefore, two different cases may be considered for each piezoelectric sublayer: applied difference of potentials (actuator) or unknown difference of potentials (sensor). Let us define the corresponding subgroups \mathbf{V}_A^e and \mathbf{V}_S^e of the elementary electrical dofs \mathbf{V}^e . Then, the vector $\hat{\mathbf{q}}_e$ in (18) may be decomposed such that $\hat{\mathbf{q}}_e = \text{col}(\mathbf{q}_e, \mathbf{V}_S^e, \mathbf{V}_A^e)$. Consequently, the system (25) becomes

$$\begin{bmatrix} \hat{\mathbf{M}}^e & \mathbf{0} & \mathbf{0} \\ \mathbf{0} & \mathbf{0} & \mathbf{0} \\ \mathbf{0} & \mathbf{0} & \mathbf{0} \end{bmatrix} \begin{bmatrix} \ddot{\mathbf{q}}_e \\ \ddot{\mathbf{V}}_S^e \\ \ddot{\mathbf{V}}_A^e \end{bmatrix} + \begin{bmatrix} \mathbf{K}_{fm}^e + \mathbf{K}_c^e & -\mathbf{K}_{fmeS}^e & -\mathbf{K}_{fmeA}^e \\ -\mathbf{K}_{fmeS}^{eT} & \mathbf{K}_{feS}^e & \mathbf{0} \\ -\mathbf{K}_{fmeA}^{eT} & \mathbf{0} & \mathbf{K}_{feA}^e \end{bmatrix} \begin{Bmatrix} \mathbf{q}_e \\ \mathbf{V}_S^e \\ \mathbf{V}_A^e \end{Bmatrix} = \begin{Bmatrix} \mathbf{F}_m^e \\ \mathbf{0} \\ \mathbf{0} \end{Bmatrix} \quad (26)$$

Since the electrical dofs \mathbf{V}_A^e are imposed, their virtual variations $\delta \mathbf{V}_A^e$ vanish. Therefore, the third equation of (26) is automatically satisfied and may be ignored. Also the corresponding term to \mathbf{V}_A^e in the first equation can be moved to the right-hand side as an equivalent electrical work, defined by

$$\mathbf{F}_e^e = \mathbf{K}_{fmeA}^e \mathbf{V}_A^e \quad (27)$$

The second equation of (26) can then be used to express the unknown potentials \mathbf{V}_S^e in terms of the mechanical dofs \mathbf{q}_e , such as

$$\mathbf{V}_S^e = \mathbf{K}_{feS}^{e-1} \mathbf{K}_{fmeS}^{eT} \mathbf{q}_e \quad (28)$$

Replacing expressions (27) and (28) in the first equation of (26) leads to the following electrical dof condensed elementary system:

$$\hat{\mathbf{M}}^e \ddot{\mathbf{q}}_e + (\mathbf{K}_{fm}^e - \mathbf{K}_{fmeS}^e \mathbf{K}_{feS}^{e-1} \mathbf{K}_{fmeS}^{eT} + \mathbf{K}_c^e) \mathbf{q}_e = \mathbf{F}_m^e + \mathbf{F}_e^e \quad (29)$$

Hence, the mechanical dofs, due to mechanical and/or electrical loads \mathbf{F}_m^e and \mathbf{F}_e^e , may be evaluated first, then unknown electrical dofs are found through a post-processing calculation using (28). This method not only leads to faster calculations since matrices dimensions are lower but also prevents ill-conditioning problems of solving directly Equation (26). Therefore, both piezoelectric actuators and sensors can be considered in a closed-loop analysis.

Then, one may assemble this elementary system to get the corresponding global mass and stiffness matrices, and mechanical and electrical load vectors, \mathbf{M} , \mathbf{K}_f , \mathbf{K}_c , \mathbf{F}_m and \mathbf{F}_e . Also, a standard viscous damping matrix \mathbf{D} may be considered *a posteriori*. Consequently, the assembled system becomes

$$\mathbf{M}\ddot{\mathbf{q}} + \mathbf{D}\dot{\mathbf{q}} + (\mathbf{K}_f + \mathbf{K}_c)\mathbf{q} = \mathbf{F}_m + \mathbf{F}_e \quad (30)$$

It is worthwhile to notice that the induced potential in the sensors due to the direct piezoelectric effect, that is the piezoelectric layers in which the electric potentials are not imposed, leads to an increase in the stiffness of these layers. This is due to an electrical load generated in the piezoelectric layer by the induced potential. Through a theoretical analysis, it can be shown that this stiffness augmentation is such that the elastic material constants $c_{11}^{*k_j}$ of the passive piezoelectric layers are replaced by new augmented elastic constants $\hat{c}_{11}^{k_j}$, for membrane and membrane-bending coupling terms, and $\hat{c}_{11}^{k_j}$, for bending terms, which are (see Appendix B)

$$\hat{c}_{11}^{k_j} = c_{11}^{*k_j} + \frac{(e_{31}^{*k_j})^2}{\epsilon_{33}^{*k_j}}, \quad \hat{c}_{11}^{k_j} = c_{11}^{*k_j} + \frac{(e_{31}^{*k_j})^2}{\epsilon_{33}^{*k_j}} \frac{\bar{I}_{k_j}^2}{A_{k_j} I_{k_j}} \quad (31)$$

VISCOELASTIC CORE FREQUENCY-DEPENDENCE MODELLING

In order to correctly model the viscoelastic core, one must take into account the frequency-dependence of its viscoelastic material. This is done here, through the Lesieutre's ADF model, which allows both frequency and time-domain analyses of highly damped structures [10]. Using the procedure presented in Reference [11], it is possible to include the viscoelastic modelling in the equations of motion (30) without needing to reformulate the finite element model. This procedure shall be briefly recalled here. Hence, supposing the viscoelastic Poisson's ratio frequency-independent, so that the shear and Young's moduli are proportional the discretized equations of motion (30) can be written as

$$\mathbf{M}\ddot{\mathbf{q}} + \mathbf{D}\dot{\mathbf{q}} + [\mathbf{K}_f + G^*(t)\bar{\mathbf{K}}_c]\mathbf{q} = \mathbf{F}_m + \mathbf{F}_e \quad (32)$$

where the condensed faces stiffness matrix of (30) is \mathbf{K}_f and the viscoelastic core stiffness is $\mathbf{K}_c = G^*(t)\bar{\mathbf{K}}_c$. $G^*(t)$ is the complex frequency-dependent shear modulus of the viscoelastic layer.

The ADF model is based on a separation of the viscoelastic material strains in an elastic part, instantaneously proportional to the stress, and an anelastic part, representing material relaxation [10]. Lesieutre and Lee [15] also suggested a finite element implementation through replacing the dofs vector \mathbf{q} by $\mathbf{q}^e = \mathbf{q} - \sum_i \mathbf{q}_i^a$ in the viscoelastic strain energy. \mathbf{q}^e and \mathbf{q}_i^a

represent the dofs vectors associated with the elastic and anelastic strains, respectively. Therefore the following systems, describing the evolution of elastic and anelastic dofs, respectively, hold:

$$\mathbf{M}\ddot{\mathbf{q}} + \mathbf{D}\dot{\mathbf{q}} + (\mathbf{K}_f + \mathbf{K}_c^\infty)\mathbf{q} - \mathbf{K}_c^\infty \sum_i \mathbf{q}_i^a = \mathbf{F}_m + \mathbf{F}_e \quad (33)$$

$$\frac{C_i}{\Omega_i} \mathbf{K}_c^\infty \dot{\mathbf{q}}_i^a - \mathbf{K}_c^\infty \mathbf{q} + C_i \mathbf{K}_c^\infty \mathbf{q}_i^a = 0 \quad (34)$$

where $\mathbf{K}_c^\infty = G_\infty \bar{\mathbf{K}}_c$, for $G_\infty = G_0(1 + \sum_i \Delta_i)$, $C_i = (1 + \sum_i \Delta_i)/\Delta_i$, and material parameters G_0 , Δ_i and Ω_i are evaluated by curve-fitting of the measurements of $G^*(\omega)$, represented as a series of functions in the frequency-domain

$$G^*(\omega) = G_0 + G_0 \sum_i \Delta_i \frac{\omega^2 + j\omega\Omega_i}{\omega^2 + \Omega_i^2} \quad (35)$$

and j states for $j = \sqrt{-1}$. Notice that there is one group of anelastic dofs \mathbf{q}_i^a for each series of functions considered. From (35), the relaxed or static modulus is clearly $G_0 = G^*(0)$. Combination of (33) and (34), leads to the following augmented system:

$$\bar{\mathbf{M}}\ddot{\bar{\mathbf{q}}} + \bar{\mathbf{D}}\dot{\bar{\mathbf{q}}} + \bar{\mathbf{K}}\bar{\mathbf{q}} = \bar{\mathbf{F}} \quad (36)$$

with

$$\begin{aligned} \bar{\mathbf{M}} &= \begin{bmatrix} \mathbf{M} & \mathbf{0} \\ \mathbf{0} & \mathbf{0} \end{bmatrix}, \quad \bar{\mathbf{D}} = \begin{bmatrix} \mathbf{D} & \mathbf{0} \\ \mathbf{0} & \mathbf{D}_{aa} \end{bmatrix}, \quad \bar{\mathbf{F}} = \begin{Bmatrix} \mathbf{F}_m + \mathbf{F}_e \\ \mathbf{0} \end{Bmatrix} \\ \bar{\mathbf{K}} &= \begin{bmatrix} \mathbf{K}_f + \mathbf{K}_c^\infty & \mathbf{K}_{ea} \\ \mathbf{K}_{ea}^T & \mathbf{K}_{aa} \end{bmatrix}, \quad \bar{\mathbf{q}} = \text{col}(\mathbf{q}, \mathbf{q}_1^a, \dots, \mathbf{q}_n^a) \end{aligned}$$

where

$$\begin{aligned} \mathbf{D}_{aa} &= \begin{bmatrix} \frac{C_1}{\Omega_1} \mathbf{K}_c^\infty & & \mathbf{0} \\ & \ddots & \\ \mathbf{0} & & \frac{C_n}{\Omega_n} \mathbf{K}_c^\infty \end{bmatrix}, \quad \mathbf{K}_{aa} = \begin{bmatrix} C_1 \mathbf{K}_c^\infty & & \mathbf{0} \\ & \ddots & \\ \mathbf{0} & & C_n \mathbf{K}_c^\infty \end{bmatrix} \\ \mathbf{K}_{ea} &= [-\mathbf{K}_c^\infty \quad \dots \quad -\mathbf{K}_c^\infty] \end{aligned}$$

After a modal decomposition $\mathbf{q}_i^a = \mathbf{T}\hat{\mathbf{q}}_i^d$ such that $\Lambda = \mathbf{T}^T \mathbf{K}_c^\infty \mathbf{T}$, the matrices \mathbf{D}_{aa} , \mathbf{K}_{aa} and \mathbf{K}_{ea} corresponding to the dissipative dofs can be written as (see Reference [11] for details)

$$\mathbf{D}_{aa} = G_\infty \text{diag} \left(\frac{C_1}{\Omega_1} \Lambda, \dots, \frac{C_n}{\Omega_n} \Lambda \right), \quad \mathbf{K}_{aa} = G_\infty \text{diag}(C_1 \Lambda, \dots, C_n \Lambda), \quad \mathbf{K}_{ea} = [-\mathbf{K}_c^\infty \mathbf{T} \quad \dots \quad -\mathbf{K}_c^\infty \mathbf{T}]$$

so that the system dimension is reduced and the matrices associated with the ADF dissipative dofs are diagonalized. Λ is a diagonal matrix containing the non-vanishing eigenvalues of the high-frequency viscoelastic stiffness matrix \mathbf{K}_c^∞ and \mathbf{T} is the corresponding eigenvectors matrix. More details on this passage may be found in Reference [11].

CONTROL ALGORITHM

For control design, the augmented equations (36) are transformed into state-space form as follows:

$$\begin{aligned} \dot{\mathbf{x}} &= \mathbf{A}\mathbf{x} + \mathbf{B}\mathbf{u} + \mathbf{p} \\ \mathbf{y} &= \mathbf{C}\mathbf{x} \end{aligned} \quad \text{with } \mathbf{x} = \begin{Bmatrix} \bar{\mathbf{q}} \\ \dot{\mathbf{q}} \end{Bmatrix} \quad (37)$$

where \mathbf{C} establishes, in terms of the state vector \mathbf{x} , the variables \mathbf{y} to be measured. \mathbf{A} , \mathbf{B} and \mathbf{p} are the system dynamics, input distribution and perturbation matrices, respectively. They are given by

$$\mathbf{A} = \begin{bmatrix} \mathbf{0} & \mathbf{0} & \cdots & \mathbf{0} & \mathbf{I} \\ \frac{\Omega_1}{C_1} \mathbf{T}^T & -\Omega_1 \mathbf{I} & & \mathbf{0} & \mathbf{0} \\ \vdots & & \ddots & & \mathbf{0} \\ \frac{\Omega_n}{C_n} \mathbf{T}^T & \mathbf{0} & & -\Omega_n \mathbf{I} & \mathbf{0} \\ -\mathbf{M}^{-1}(\mathbf{K}_p + \mathbf{K}_c^\infty) & \mathbf{M}^{-1} \mathbf{K}_c^\infty \mathbf{T} & \cdots & \mathbf{M}^{-1} \mathbf{K}_c^\infty \mathbf{T} & -\mathbf{M}^{-1} \mathbf{D} \end{bmatrix} \quad (38)$$

$$\mathbf{B} = \begin{bmatrix} \mathbf{0} \\ \mathbf{0} \\ \mathbf{M}^{-1} \mathbf{F}_e^* \end{bmatrix}, \quad \mathbf{p} = \begin{bmatrix} \mathbf{0} \\ \mathbf{0} \\ \mathbf{M}^{-1} \mathbf{F}_m \end{bmatrix}$$

The potential factored-out piezoelectric force vector \mathbf{F}_e^* is defined as the piezoelectric force \mathbf{F}_e for a unit applied voltage on the corresponding actuator.

The system matrices in (37) are, generally, too large for use in the control design. Hence, they are reduced further using $\mathbf{x} = \mathbf{T}_r \hat{\mathbf{x}}$, where the complex right eigenvector matrix \mathbf{T}_r of the system matrix \mathbf{A} , and its corresponding left counterpart \mathbf{T}_l , are the solution of

$$\mathbf{A} \mathbf{T}_r = \Lambda \mathbf{T}_r, \quad \mathbf{A}^T \mathbf{T}_l = \Lambda \mathbf{T}_l \quad (39)$$

normalized by $\mathbf{T}_l^T \mathbf{T}_r = \mathbf{I}$. The overdamped modes, corresponding to the dissipative dofs, are eliminated and some elastic modes are retained, leading to a reduced state vector $\hat{\mathbf{x}}$. Thus, the reduced state-space system of (37) is

$$\dot{\hat{\mathbf{x}}} = \hat{\mathbf{A}} \hat{\mathbf{x}} + \hat{\mathbf{B}} \mathbf{u} + \hat{\mathbf{p}}, \quad \mathbf{y} = \hat{\mathbf{C}} \hat{\mathbf{x}} \quad (40)$$

where

$$\hat{\mathbf{A}} = \mathbf{T}_l^T \mathbf{A} \mathbf{T}_r, \quad \hat{\mathbf{B}} = \mathbf{T}_l^T \mathbf{B}, \quad \hat{\mathbf{p}} = \mathbf{T}_l^T \mathbf{p}, \quad \hat{\mathbf{C}} = \mathbf{C} \mathbf{T}_r$$

A full state feedback control $\mathbf{u} = -\mathbf{K}_g \hat{\mathbf{x}}$ is considered. Replacing this control law in (40), the following control system is obtained:

$$\dot{\hat{\mathbf{x}}} = (\hat{\mathbf{A}} - \hat{\mathbf{B}} \mathbf{K}_g) \hat{\mathbf{x}} + \hat{\mathbf{p}}, \quad \mathbf{y} = \hat{\mathbf{C}} \hat{\mathbf{x}} \quad (41)$$

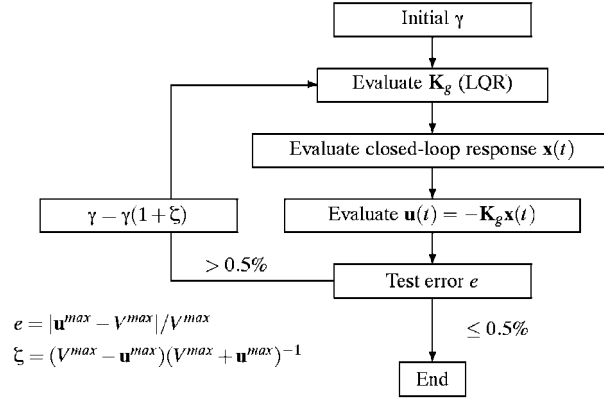


Figure 3. Optimal control design under voltage constraint V^{max} .

An iterative linear quadratic regulator (LQR) optimal control algorithm, modified from that developed in Reference [14], is used for \mathbf{K}_g evaluation, under limited maximum beam tip deflection and difference of electric potential applied to the piezoelectric actuator. That is, the LQR weight matrices are considered as \mathbf{Q} and $\mathbf{R} = \gamma \mathbf{I}$, γ being evaluated to respect maximum beam deflection and control voltage. The algorithm is shown in Figure 3.

Notice that, here, the factor γ controls the input weight matrix \mathbf{R} , and not the state one \mathbf{Q} as in Reference [14], although the concept is equivalent.

CONCLUSIONS

An electromechanically coupled finite element model to handle active–passive damped multi-layer sandwich beams was presented. Classical laminate theory was used to model the multi-layer piezoelectric faces, whereas classical sandwich theory was considered for the laminate piezoelectric face/viscoelastic core/laminate piezoelectric face beam, leading to three-layer kinematic description and layerwise material constitutive equations. This has resulted in additional membrane-bending coupling terms in electromechanical internal and external forces and translation–rotation coupling terms in inertial forces. The finite element was implemented assuming Lagrange linear shape functions for the mean and relative axial displacements and Hermite cubic ones for the transverse deflection. The differences of electric potentials of the piezoelectric layers were assumed constant in the element. This yielded eight mechanical dofs and one electrical dof per piezoelectric layer. It was shown that sensor voltages can be either considered as electrical dofs or evaluated through post-processing of mechanical results. When using electrical dofs, these were condensed at the elementary level, leading to a modified eight mechanical dofs finite element.

The viscoelastic core was modelled through Lesieutre’s ADF time-domain model to account for frequency-dependent properties of such material. This has resulted in an augmented state-space system capable of well representing, even in time-domain analyses, the frequency-dependence of highly damped beams. The problem of increase in the system dimension, due to the additional ADF internal variables, was solved through a complex-basis model reduction

of the augmented state-space system. The reduced system was then applied to the active–passive constrained optimal control of sandwich damped beams, using an iterative control algorithm to account for input constraints.

In the second part of this paper, this piezo–visco–elastic finite element model will be validated through comparisons with analytical, numerical and experimental results found in the literature. Then, the performance of the hybrid active–passive control system will be evaluated through the active control of a viscoelastically damped cantilever sandwich beam.

The present finite element model has been extended to take into account the viscoelastic material temperature-dependence effect [16] and optimization procedures are to be implemented. Also, this model was used to compare the performance of several control algorithms [17].

APPENDIX A. FINITE ELEMENT INTERPOLATION AND DEFORMATION MATRICES

Lagrange linear and Hermite cubic shape functions were considered for the axial displacements and deflection, respectively. Therefore, the generalized displacements vector $\mathbf{d} = \text{col}(\tilde{u}, w, \tilde{u})$, are discretized as

$$\mathbf{d} = \hat{\mathbf{N}}_d \hat{\mathbf{q}}_e$$

where

$$\hat{\mathbf{N}}_d = \begin{bmatrix} N_1 & 0 & 0 & 0 & | & N_2 & 0 & 0 & 0 & | & 0 & \dots & 0 \\ 0 & N_3 & N_4 & 0 & | & 0 & N_5 & N_6 & 0 & | & 0 & \dots & 0 \\ 0 & 0 & 0 & N_1 & | & 0 & 0 & 0 & N_2 & | & 0 & \dots & 0 \end{bmatrix}$$

with $\hat{\mathbf{q}}_e$ the dofs vector defined in (18) and N_l ($l=1, \dots, 6$) being the following standard shape functions:

$$N_1 = 1 - \frac{x}{L_e}, \quad N_2 = \frac{x}{L_e}, \quad N_3 = 1 - \frac{3x^2}{L_e^2} + \frac{2x^3}{L_e^3}$$

$$N_4 = x \left(1 - \frac{x}{L_e}\right)^2, \quad N_5 = \frac{x^2}{L_e^2} \left(3 - \frac{2x}{L_e}\right), \quad N_6 = \frac{x^2}{L_e} \left(\frac{x}{L_e} - 1\right)$$

The differences of electric potentials in the faces sublayers are discretized as

$$V_{k_j} = \hat{\mathbf{N}}_{pk_j} \hat{\mathbf{q}}_e$$

where the interpolation matrices $\hat{\mathbf{N}}_{pk_j}$ are

$$\begin{bmatrix} \hat{\mathbf{N}}_{pa_1} \\ \vdots \\ \hat{\mathbf{N}}_{pa_{\hat{i}}} \\ \hat{\mathbf{N}}_{pb_1} \\ \vdots \\ \hat{\mathbf{N}}_{pb_{\hat{i}}} \end{bmatrix} = \begin{bmatrix} 0 & 0 & 0 & 0 & 0 & 0 & 0 & 0 & 1 & & 0 & 0 & 0 \\ \vdots & & & & & & & & & \ddots & & & \vdots \\ 0 & 0 & 0 & 0 & 0 & 0 & 0 & 0 & 0 & & 1 & 0 & 0 \\ 0 & 0 & 0 & 0 & 0 & 0 & 0 & 0 & 0 & & 0 & 1 & 0 \\ \vdots & & & & & & & & & \ddots & & & \vdots \\ 0 & 0 & 0 & 0 & 0 & 0 & 0 & 0 & 0 & & 0 & 0 & 1 \end{bmatrix}$$

Then, to discretize the displacements of each layer of the beam (3), separate interpolation matrices are introduced. Those corresponding to the translation in x and z directions and rotation are the following:

$$\begin{aligned} \mathbf{N}_{kx} &= [N_1 \quad 0 \quad 0 \quad \pm \frac{1}{2}N_1 \mid N_2 \quad 0 \quad 0 \quad \pm \frac{1}{2}N_2 \mid 0 \quad \cdots \quad 0], \quad k = a(+), b(-) \\ \mathbf{N}_{cx} &= [N_1 \quad dN'_3 \quad dN'_4 \quad 0 \mid N_2 \quad dN'_5 \quad dN'_6 \quad 0 \mid 0 \quad \cdots \quad 0] \\ \mathbf{N}_{kr} &= [0 \quad -N'_3 \quad -N'_4 \quad 0 \mid 0 \quad -N'_5 \quad -N'_6 \quad 0 \mid 0 \quad \cdots \quad 0], \quad k = a(+), b(-) \\ \mathbf{N}_{cz} &= [0 \quad \lambda N'_3 \quad \lambda N'_4 \quad \frac{1}{h_c}N_1 \mid 0 \quad \lambda N'_5 \quad \lambda N'_6 \quad \frac{1}{h_c}N_2 \mid 0 \quad \cdots \quad 0] \\ \mathbf{N}_z &= [0 \quad N_3 \quad N_4 \quad 0 \mid 0 \quad N_5 \quad N_6 \quad 0 \mid 0 \quad \cdots \quad 0] \end{aligned}$$

Starting from relations (4) and using these displacements interpolation matrices, the faces (k) and core (c), membrane (m) and bending (b) strain operators are written as

$$\begin{aligned} \mathbf{B}_{km} &= [N'_1 \quad 0 \quad 0 \quad \pm \frac{1}{2}N'_1 \mid N'_2 \quad 0 \quad 0 \quad \pm \frac{1}{2}N'_2 \mid 0 \quad \cdots \quad 0], \quad k = a(+), b(-) \\ \mathbf{B}_{cm} &= [N'_1 \quad dN''_3 \quad dN''_4 \quad 0 \mid N'_2 \quad dN''_5 \quad dN''_6 \quad 0 \mid 0 \quad \cdots \quad 0] \\ \mathbf{B}_{kb} &= [0 \quad -N''_3 \quad -N''_4 \quad 0 \mid 0 \quad -N''_5 \quad -N''_6 \quad 0 \mid 0 \quad \cdots \quad 0], \quad k = a(+), b(-) \\ \mathbf{B}_{cb} &= [0 \quad \lambda N''_3 \quad \lambda N''_4 \quad \frac{1}{h_c}N'_1 \mid 0 \quad \lambda N''_5 \quad \lambda N''_6 \quad \frac{1}{h_c}N'_2 \mid 0 \quad \cdots \quad 0] \end{aligned}$$

Shear strains are only considered in the core which are represented by the following operator:

$$\mathbf{B}_{cs} = [0 \quad (\lambda + 1)N'_3 \quad (\lambda + 1)N'_4 \quad \frac{1}{h_c}N_1 \mid 0 \quad (\lambda + 1)N'_5 \quad (\lambda + 1)N'_6 \quad \frac{1}{h_c}N_2 \mid 0 \quad \cdots \quad 0]$$

APPENDIX B. PIEZOELECTRIC STIFFNESS AUGMENTATION DUE TO INDUCED POTENTIALS

From the terms of (9) corresponding to δV_{k_j} and noting that no terms relative to such variations are present neither in (14) nor in (16), the variational formulation (7) results, for the electric

potential variation δV_{k_j} of the k_j th face piezoelectric sublayer, in

$$e_{31}^{*k_j} (A_{k_j} \varepsilon_k^m + \bar{I}_{k_j} \varepsilon_k^b) - \epsilon_{33}^{*k_j} A_{k_j} \frac{V_{k_j}}{h_{k_j}} = 0$$

leading to

$$\frac{V_{k_j}}{h_{k_j}} = \frac{e_{31}^{*k_j}}{\epsilon_{33}^{*k_j}} \left(\varepsilon_k^m + \frac{\bar{I}_{k_j}}{A_{k_j}} \varepsilon_k^b \right)$$

Substitution of this result in (9) leads, for a known difference of potential ($\delta V_{k_j} = 0$), to

$$\begin{aligned} \delta \tilde{H}_{k_j} = \int_0^L & \left\{ c_{11}^{*k_j} [A_{k_j} \delta \varepsilon_k^m \varepsilon_k^m + \bar{I}_{k_j} (\delta \varepsilon_k^m \varepsilon_k^b + \delta \varepsilon_k^b \varepsilon_k^m) + I_{k_j} \delta \varepsilon_k^b \varepsilon_k^b] \right. \\ & \left. + \frac{e_{31}^{*k_j 2}}{\epsilon_{33}^{*k_j}} \left[A_{k_j} \delta \varepsilon_k^m \varepsilon_k^m + \bar{I}_{k_j} (\delta \varepsilon_k^m \varepsilon_k^b + \delta \varepsilon_k^b \varepsilon_k^m) + \frac{\bar{I}_{k_j}^2}{A_{k_j}} \delta \varepsilon_k^b \varepsilon_k^b \right] \right\} dx \end{aligned}$$

or, introducing two new modified elastic constants $\bar{c}_{11}^{k_j}$ and $\hat{c}_{11}^{k_j}$,

$$\delta \tilde{H}_{k_j} = \int_0^L \left\{ \bar{c}_{11}^{k_j} [A_{k_j} \delta \varepsilon_k^m \varepsilon_k^m + \bar{I}_{k_j} (\delta \varepsilon_k^m \varepsilon_k^b + \delta \varepsilon_k^b \varepsilon_k^m)] + \hat{c}_{11}^{k_j} I_{k_j} \delta \varepsilon_k^b \varepsilon_k^b \right\} dx$$

where these modified constants are given in (31).

APPENDIX C. NOMENCLATURE

A_i	cross-sectional area of the layer i
\mathbf{A}	state-space system matrix
$\hat{\mathbf{A}}$	reduced state-space system matrix
a	piezoelectric actuators length
\mathbf{B}	state-space control input matrix
$\hat{\mathbf{B}}$	reduced state-space control input matrix
\mathbf{B}_{im}	i th layer membrane strain interpolation matrix
\mathbf{B}_{ib}	i th layer bending strain interpolation matrix
\mathbf{B}_{cs}	core shear strain interpolation matrix
b, L	beam width and length, respectively
\mathbf{C}	state-space output matrix
$\hat{\mathbf{C}}$	reduced state-space output matrix
C_i	ADF viscoelastic material parameter of the i th series

$c_{ij}, e_{lj}, \epsilon_{ll}$	elastic, piezoelectric and dielectric constants, respectively
\mathbf{D}	viscous damping matrix
$\bar{\mathbf{D}}$	ADF augmented damping matrix
Δ_i	ADF viscoelastic material parameter of the i th series
d	membrane-bending coupling parameter
dof	degrees of freedom
δH	virtual work of electromechanical internal forces
δT	virtual work of inertial forces
δW	virtual work of external forces
E_3, D_3	transverse electrical field and displacement, respectively
ϵ_i^b	bending strain of layer i
ϵ_i^m	axial strain at centreline of layer i (membrane strain)
$\epsilon_c^s, \epsilon_{5c}$	shear strain of layer c
ϵ_{1i}	axial strain of layer i
\mathbf{F}_m	mechanical loads vector
\mathbf{F}_e	induced electrical loads vector
G^*	viscoelastic core frequency-dependent complex shear modulus
G_0	viscoelastic core relaxed (static) shear modulus
G_∞	viscoelastic core unrelaxed shear modulus
γ	LQR state ponderation factor
h_i	thickness of layer i
h_v	thickness of viscoelastic layer
I_i	cross-section second moment area of the layer i
\bar{I}_i	cross-section first moment area of the layer i
$\bar{\mathbf{K}}$	ADF augmented stiffness matrix
\mathbf{K}_c	core stiffness matrix
\mathbf{K}_c^∞	unrelaxed core stiffness matrix
\mathbf{K}_f	faces stiffness matrix
$\hat{\mathbf{K}}_{kjm}^e$	elementary mechanical stiffness matrix
$\hat{\mathbf{K}}_{k_j m e}^e$	elementary piezoelectric stiffness matrix
$\hat{\mathbf{K}}_{k_j e}^e$	elementary dielectric stiffness matrix
\mathbf{K}_g	control gain matrix
λ	relative shear-bending coupling parameter
\mathbf{M}	mass matrix
$\bar{\mathbf{M}}$	ADF augmented mass matrix
N_i, M_i, Q_i	point normal, moment and shear resultants on layer i , respectively
n_i, m_i, q_i	distributed normal, moment and shear resultants on layer i , respectively
\mathbf{N}_{ix}	translation in x direction interpolation matrix for i th layer
\mathbf{N}_{ir}	rotation interpolation matrix for i th layer
\mathbf{N}_z	translation in z direction interpolation matrix
\mathbf{N}_{pk_j}	k_j sublayer difference of electric potential interpolation matrix
Ω_i	ADF viscoelastic material parameter of the i th series
\mathbf{p}	state-space perturbation vector
\mathbf{Q}	LQR state ponderation matrix
\mathbf{q}	dofs vector

$\bar{\mathbf{q}}$	ADF augmented dofs vector
\mathbf{q}^e	elastic dofs vector
\mathbf{q}_i^a	i th anelastic dofs vector
\mathbf{q}_e	elementary mechanical dofs vector
$\hat{\mathbf{q}}_e$	elementary dofs vector
\mathbf{R}	LQR input ponderation matrix
ρ_i	mass density of the layer i
σ_1, σ_5	axial and shear stresses, respectively
$\mathbf{T}_l, \mathbf{T}_r$	left and right state-space complex eigenvectors matrices
\mathbf{u}	control input vector
\tilde{u}	mean of the axial displacements of surface layers centrelines
\tilde{u}	difference between the axial displacements of surface layers centrelines
$\tilde{u}_1, \tilde{u}'_1, w_1, w'_1$	mean and relative axial faces displacements, transverse deflection and its derivative for element node 1
$\tilde{u}_2, \tilde{u}'_2, w_2, w'_2$	mean and relative axial faces displacements, transverse deflection and its derivative for element node 2
u_i	axial displacement of the centreline of the layer i
\tilde{u}_i	axial displacement of the layer i
\mathbf{V}_A^e	applied (actuator) elementary electric dofs vector
\mathbf{V}_S^e	unknown (sensor) elementary electric dofs vector
V_{k_j}	difference of electric potentials on the sublayer k_j
$V_{k_j}^+, V_{k_j}^-$	electric potentials at the top and bottom skins of the sublayer k_j , respectively
w	transverse displacement of beam centreline
\mathbf{x}	state vector
$\hat{\mathbf{x}}$	reduced state vector
x, z	axial and transverse coordinates
\mathbf{y}	state-space output vector
z_k	distance to centreline of surface layer k ($k = a, b$)
z_{k_j}	distance to centreline of face sublayer k_j

Subscripts

c	states for quantities related to sandwich core
f	states for quantities related to sandwich surface layers
i	states for beam layers a, b or c
j	states for faces sublayers
k	states for surface layers a or b
m	states for mechanical contributions

Superscripts

*	states for modified material constants
b	states for bending contributions
c	states for core material constants
f	states for surface layers material constants
m	states for membrane contributions
s	states for shear contributions

ACKNOWLEDGEMENTS

Support of the 'Délégation Générale pour l'Armement'—Advanced Materials Branch, under contract D.G.A./D.S.P./S.T.T.C./MA. 97-2530, is gratefully acknowledged. The first author acknowledges also the support of the Brazilian government (CAPES) through a doctoral scholarship award number BEX 2494/95-7.

REFERENCES

1. Benjeddou A. Advances in hybrid active-passive vibration and noise control via piezoelectric and viscoelastic materials. *Journal of Vibration and Control* 2000; to appear.
2. Inman DJ, Lam MJ. Active constrained layer damping treatments. In *6th International Conference on Recent Advances in Structural Dynamics*, vol. 1, Ferguson NS, Wolfe HF, Mei C (eds). Southampton, UK, 1997; 1–20.
3. Baz A, Ro J. Performance characteristics of active constrained layer damping. *Shock and Vibration* 1995; **2**(1): 33–42.
4. Crassidis J, Baz A, Wereley N. H_∞ control of active constrained layer damping. In *11th Symposium on Structural Dynamics and Control*, Blacksburg, VA, May 1997.
5. Rongong JA, Wright JR, Wynne RJ, Tomlinson GR. Modelling of a hybrid constrained layer/piezoceramic approach to active damping. *Journal of Vibration and Acoustics* 1997; **119**(1):120–130.
6. Chen T, Baz A. Performance characteristics of active constrained layer damping versus passive constrained layer damping with active control. In: *Smart Structures and Materials 1996: Mathematics and Control in Smart Structures*, vol. 2715, Varadan VV, Chandra J (eds). SPIE: Bellingham, USA, 1996; 256–268.
7. Lam MJ, Inman DJ, Saunders WR. Vibration control through passive constrained layer damping and active control. *Journal of Intelligent Material Systems and Structures* 1997; **8**(8):663–677.
8. Benjeddou A, Trindade MA, Ohayon R. A unified beam finite element model for extension and shear piezoelectric actuation mechanisms. *Journal of Intelligent Material Systems and Structures* 1997; **8**(12): 1012–1025.
9. Benjeddou A, Trindade MA, Ohayon R. New shear actuated smart structure beam finite element. *AIAA Journal* 1999; **37**(3):378–383.
10. Lesieutre GA, Bianchini E. Time domain modeling of linear viscoelasticity using anelastic displacement fields. *Journal of Vibration and Acoustics* 1995; **117**(4):424–430.
11. Trindade MA, Benjeddou A, Ohayon R. Modeling of frequency-dependent viscoelastic materials for active-passive vibration damping. *Journal of Vibration and Acoustics* 2000; **122**(2):169–174.
12. Rahmoune M, Benjeddou A, Ohayon R, Osmont D. New thin piezoelectric plate models. *Journal of Intelligent Material Systems and Structures* 1998; **9**(12):1017–1029.
13. Benjeddou A, Trindade MA, Ohayon R. Piezoelectric actuation mechanisms for intelligent sandwich structures. *Smart Material and Structures* 2000; **9**(3):328–335.
14. Trindade MA, Benjeddou A, Ohayon R. Parametric analysis of the vibration control of sandwich beams through shear-based piezoelectric actuation. *Journal of Intelligent Material Systems and Structures* 1999; **10**(5): 377–385.
15. Lesieutre GA, Lee U. A finite element for beams having segmented active constrained layers with frequency-dependent viscoelastics. *Smart Materials and Structures* 1996; **5**(5):615–627.
16. Trindade MA, Benjeddou A, Ohayon R. Finite element analysis of frequency- and temperature-dependent hybrid active-passive vibration damping. *Revue Européenne des Éléments Finis* 2000; **9**(1–3):89–111.
17. Trindade MA, Benjeddou A, Ohayon R. Piezoelectric active vibration control of sandwich damped beams. *Journal of Sound and Vibration* 2000; to appear.